Chinese Journal of Electronics
vol. 33, no. 2, pp. 456–462, March 2024
https://doi.org/10.23919/cje.2023.00.057

RESEARCH ARTICLE

Miniaturized, Wide Stopband Filter Based on Shielded Capacitively Loaded SIW Resonators

Yan ZHENG, Hanyu TIAN, and Yuandan DONG

University of Electronic Science and Technology of China (UESTC), Chengdu 611731, China

Corresponding author: Yuandan DONG, Email: ydong@uestc.edu.cn
Manuscript Received February 24, 2023; Accepted June 5, 2023

Abstract — Based on the full-mode capacitively loaded substrate integrated waveguide (SIW) resonator and the miniaturized shielded half-mode capacitively loaded SIW (S-HMCSIW) cavities, a novel compact high-performance filter is proposed. The footprint of the half-mode SIW (HMSIW) is further reduced due to the application of the capacitive-loading technique. By applying cross coupling, the proposed SIW filter's transmission zero enhances the stopband rejection and shows excellent selectivity. For the bandpass filter, the measured $|S_{21}|$ and $|S_{11}|$ are better than 1.09 dB and −14 dB, respectively. And a 3-dB fractional bandwidth (FBW) of 9.14–10.76 GHz (FBW=16.2%) is also observed. The filter achieves a wide stopband with a −20 dB out-of-band rejection up to $2.69f_0$ ($f_0 = 10$ GHz), with a size of $0.39\lambda_g \times 0.51\lambda_g$ only. Good agreement between measurement and simulation is obtained.
Keywords — Bandpass filter, Capacitively loaded, Compact filter, Shielded cavity, Substrate integrated waveguide (SIW).
Citation — Yan ZHENG, Hanyu TIAN, and Yuandan DONG, "Miniaturized, Wide Stopband Filter Based on Shielded Capacitively Loaded SIW Resonators," *Chinese Journal of Electronics*, vol. 33, no. 2, pp. 456–462, 2024. doi: 10.23919/cje.2023.00.057.

I. Introduction

X-band bandpass filter is a crucial component for the RF front-end. It can filter the out-of-band interference and noise to satisfy the communication protocols' signal-to-noise ratio specification for RF systems, which is critical for space research and broadcast satellites. Additionally, the substrate integrated waveguide (SIW), as a unique waveguide structure, provides the benefits from both the waveguide and microstrip lines, including greater quality factor, larger power capacity, lower radiation loss, and easier integration with planar circuits. SIW is utilized in a variety of applications. However, the conventional SIW shows the drawbacks of large size and close higher-order mode effect. Consequently, there is a significant need or tendency toward the development of X-band SIW filters with a compact size, broad stopband, and low loss.

Numerous miniaturization strategies for the SIW filters have been proposed [1]–[15]. The size can be decreased effectively by introducing multiple modes on a single resonant unit [1]–[5]. It is a common practice to move the low frequency modes to higher order modes to create a multi-pole or a multi-passband response. However, this methodology is typically accompanied with the drawbacks of poor band rejection and a complicated design. A partial mode cavity can be constructed by bisecting the SIW cavity longitudinally, which can at least cut the cavity's size in half [6], [8]. Despite the merit of great size reduction, the increase of radiation losses restricts their application. Moreover, etching a particular structure onto the surface of the SIW cavity to reduce its cut-off frequency [9], [10], such as a defected ground structure (DGS) or the suggested complementary split-ring resonators (CSRRs), are additional methods for achieving downsizing. However, those approaches have a high insertion loss due to the high radiation loss. Another strategy for SIW miniaturization utilizes ridged half-mode SIW (RHMSIW) technology. By combining the half-mode format with continuous capacitive loading along the open side of the waveguide, it enables substantial miniaturizations of at least 75% while limiting the radiation losses at the cutoff [11], [12]. The multi-layered construction of SIW, which minimizes the lateral dimensions by stacking cavi-

Associate Editor: Prof. Yongle WU, Beijing University of Posts and Telecommunications

ties vertically [13]–[15], is an additional effective miniaturization technique. However, both above techniques provide additional design challenges and are difficult to integrate with the flat circuit architectures.

To obtain bandpass filters with a wide stopband based on the SIW structure, numerous methods have been proposed [16]–[25]. A cascaded low-pass filter can successfully suppress the spurious modes of the SIW filter [16], but at the cost of increasing the size of the circuit and the insertion loss. Selecting the appropriate excitation ports for SIW cavities is another useful method [17]. In [18], [19], a hybrid structure was created by merging the microstrip resonators and SIW cavities to realize a compact bandpass filter (BPF) with high selectivity. Recently, microstrip or substrate integrated defected ground structure (SIDGS)-based BPFs with wide stopband have been demonstrated [20]–[25]. However, these techniques are frequently associated with decreased flexibility or increased insertion loss.

In this work, by combining the shielded half-mode capacitively loaded SIW (S-HMCSIW) resonator and the full-mode capacitively loaded SIW resonator, a X-band compact wideband bandpass filter with a wide stopband is developed. The experimental results indicate that the stopband can be effectively extended to $2.69f_0$.

II. Analysis of S-HMCSIW Resonator

A standard square SIW cavity resonator is shown in Figure 1(a), and a capacitively loaded cavity made of the same material is illustrated in Figure 1(b) with an identical resonant frequency. They are operated in TE_{101} mode and the evanescent-mode, respectively. The resonator in Figure 1(b) utilizes two layers of closely assembled RT/Duroid 5880 material substrates with thicknesses of 10 and 20 mils, respectively. Unlike the conventional square cavity, the capacitively loaded SIW resonator in Figure 1(b) is embedded with a circular metal patch and has a ring of metalized through-holes connected to the metal patch on one side and ground on the other.

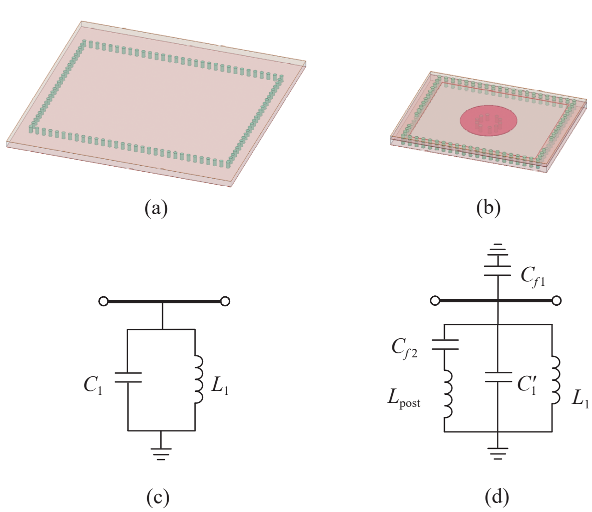

Figure 1 (a) The conventional square SIW resonator; (b) The capacitively loaded SIW resonator; (c) The equivalent circuit for the conventional square SIW resonator; (d) The equivalent circuit for the proposed capacitively loaded SIW resonator.

The equation (1) illustrates how the size and operating mode of the square SIW cavity resonator determine the resonance frequency [22].

$$f_{\mathrm{TE}_{m0n}} = \frac{c}{2\sqrt{\mu_r \varepsilon_r}} \sqrt{\left(\frac{m}{l_{\text{eff}}}\right)^2 + \left(\frac{n}{l_{\text{eff}}}\right)^2} \tag{1}$$

In the above equation, μ_r and ε_r denote the permeability and permittivity of this dielectric substrate, respectively. c is the light velocity in vacuum, l_{eff} indicates the effective waveguide length of the SIW square cavity. As shown in Figures 1(c) and (d), equivalent circuits are used to demonstrate the miniaturization principle of the capacitively loaded SIW cavity resonator in the following sections.

Innovatively, the SIW cavity resonator is equivalent to a capacitor and an inductor connected in parallel to ground, as shown by Figure 1(c), then the resonant frequency of this resonant unit is

$$f_{r1} = \frac{1}{2 \quad \sqrt{L_1 C_1}} \tag{2}$$

where the value of capacitance C_1 can be obtained by using the calculation of flat capacitance:

$$C_1 = \frac{\varepsilon_r S}{h} \tag{3}$$

where h denotes the substrate thickness of the SIW cavity, and S represents the squared-off area of the upper and lower metal layers of the SIW cavity. For convenience, define $S = l_{\text{eff}}^2$ for the square regular SIW cavity. Letting $f_{\mathrm{TE}_{m0n}}$ equal f_r gives

$$L_1 = \frac{\mu_r h l_{\text{eff}}^2}{2c^2\pi^2 l} \tag{4}$$

where l denotes actual physical length of the conventional SIW cavity. Figure 1(d) shows the equivalent circuit of the capacitively loaded SIW resonator, where C_{f1} and C_{f2} denote the flat capacitance between the patch sheet and the top copper layer of the cavity, L_{post} indicates the equivalent inductance between the metal sheet and ground, C_1' is the rest capacitance of the cavity. Then the value of C_{f1} and C_{f2} can be driven as

$$C_{f1} = \frac{\varepsilon_r \pi d_3^2}{h_1} \tag{5}$$

$$C_{f2} = \frac{\varepsilon_r \pi d_3^2}{h_2} \tag{6}$$

where, h_1 and h_2 represent the height of the upper and down substrate, respectively. L_{post} can be denoted as

$$L_{\text{post}} \approx \frac{5.08h_2}{n}\left[\ln\left(\frac{4h_2}{d_{r1}}\right)+1\right] \tag{7}$$

where, n denotes the quantity of the metalized through-holes connecting the metal sheet to the ground. Hence, the capacitively loaded SIW resonator will resonate when the imaginary part of the input admittance in Figure 1(d) equals 0, as

$$\frac{1}{L_1} - \omega^2\left(C_1' + C_{f1}\right) + \frac{j\omega C_{f2}}{1-\omega^2 L_{\text{post}} C_{f2}} = 0 \tag{8}$$

In Figure 2, three forms of resonators based on the capacitively loaded SIW cavity are presented. Type II is based on Type I, which splits along the strongest part of its electric field and reduces its size by half, but is accompanied by a larger radiation loss. Type III is built on Type II, which adds an electric wall along its strongest electric field. This reduces the radiation loss and improves the quality factor.

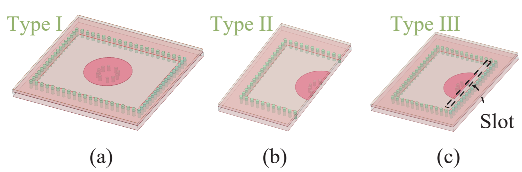

Figure 2 Three forms of resonators based on the capacitively loaded SIW cavity. (a) Type I: The capacitively loaded SIW resonator; (b) Type II is based on Type I: The half mode capacitively loaded SIW (HMCSIW) resonator; (c) Type III is built on Type II: The shielded HMCSIW (S-HMCSIW) resonator.

To show the characteristics of the three resonant units more intuitively, we compare them in terms of the unloaded quality factor (Q_{u}) and miniaturization factor (MF), where, referring to [22], the MF of a particular resonator can be calculated as

$$\text{Miniaturization factor } (\%) = 100 \times \frac{A_{\text{SIW},f_0} - A_c}{A_{\text{SIW},f_0}} \tag{9}$$

In the above equation, A_{SIW,f_0} denotes the area of the conventional SIW cavity and A_c is the area of the miniaturized resonate unit. According to the analysis of the equivalent circuit, it is known that the resonant frequency of the capacitively loaded SIW resonant unit will be affected when changing the size of the circular metal and the parameters of the metallized through-holes. Therefore, the performance of the three types of resonators is analyzed by keeping the same dimensions in the paper. As shown in Table 1, the comparison about unloaded quality factor (Q_{u}) and MF (miniaturization factor) between three types of resonators is displayed. The Q_{u} of the Type I resonator is much higher than the other two resonators, but only a small MF of 66.98% was achieved. Although slightly increased in size compared to Type II, Type III has a higher Q_{u} and is the most desirable candidate for building filters when compared to the other two resonators, which will result in low loss filters.

Table 1 Characteristic of the resonators

Resonator	Q_{u}	MF (miniaturization factor)
Type I	434	66.98%
Type II	403	83.49%
Type III	422	80.56%

III. Design Theory

1. Configuration of the proposed filter

Based on the proposed S-HMCSIW resonator, a compact filter is developed and implemented. The third-order filter worked in X-band is obtained by two S-HMCSIW resonators and a full mode capacitively loaded SIW resonator. Figure 3(a) depicts the structure in perspective, which is composed of two substrate layers and three copper layers. The adjacent metalized via-holes penetrate two substrate layers to generate the enclosed cavities. In addition, the third copper layer serves as the design's ground.

The topology scheme was displayed in Figure 3(b), where the Resonator I (R1) and Resonator III (R3) represent the S-HMCSIW resonators and Resonator II (R2) indicates the full mode capacitively loaded SIW resonator. The dominant coupling of this design is the magnetic coupling because it couples the signal at the strongest magnetic field of the S-HMSIW resonators. Furthermore, the filter introduces cross-coupling to generate transmission zero, which enhances the roll-off slope of the passband and improves the out-band suppression. It is worth noting that the size of the coupling window is a key factor in controlling the coupling and the position of transmission zero.

2. Design process and analysis

From the analysis in Section II, the relationship between the resonant frequency and the capacitively loaded SIW resonator's dimensional parameters can be obtained.

Then, from the design point of view, the center frequency of the third-order filter is set at 10 GHz and is accompanied by a 20 dB return loss with a bandwidth of 16.2%. Therefore, the coupling matrix of $N+2$ order ($N=3$) can be derived as

$$\begin{bmatrix} 0 & 1.082 & 0 & 0 & 0 \\ 1.082 & 0.032 & 1.024 & 0.127 & 0 \\ 0 & 1.024 & -0.124 & 1.024 & 0 \\ 0 & 0.127 & 1.024 & 0.032 & 1.082 \\ 0 & 0 & 0 & 1.082 & 0 \end{bmatrix} \tag{10}$$

According to the matrix (10), the quality factor Q_{e} is [22]

$$Q_{\text{e}} = \frac{\omega_0 \cdot \tau_{S11}\left(\omega_0\right)}{4} \tag{11}$$

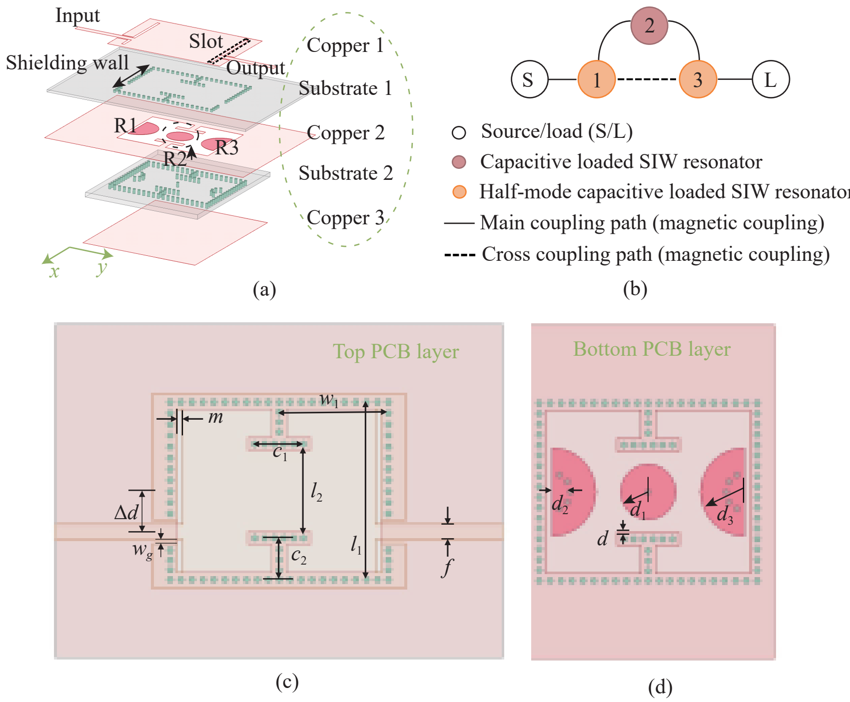

Figure 3 Configuration of the proposed structure. (a) Perspective view; (b) Its coupling schematic topology; and Its upper (c) and lower (d) PCB layers (each includes the up and down circuit metal layers).

where, $\tau_{S11}(\omega_0)$ denotes the group delay at the angular frequency ω_0. The Q_e curves for the designed filter can be seen in Figure 4. For a given microstrip-to-CPW transition, the position of the feeding line (Δd) and the size of the slot gap (w_g) influence the $Q_{e.}$ The Q_e increases by enlarging the slot gap or keeping the feed line away from the strongest part of the electric field. As shown in Figure 4(b), the coupling coefficients k_{ij} can be adjusted by tunning the value of c_1 and $l_{2.}$ For k_{12} and k_{23}, the length of the coupling window is the most influential factor. When the coupling window length c_1 increase, coupling (k_{12} & k_{23}) between adjacent resonators will decrease. And the slot width l_2 is the key parameter affecting the cross-coupling coefficient. When the slot width l_2 between the coupling windows is increased, the magnetic cross-coupling would become stronger, accompanied by the generation of the transmission zero.

Figure 5 illustrates this design principle from the field perspective. As shown in Figure 5(a), at different phase of the center frequency, resonance occurs in two types of resonators. From the perspective of the magnetic field displayed in Figure 5(b), it is evident that all the structure's resonant units are coupled magnetically at the fundamental frequency f_0. At f_{TZ} (14.36 GHz), the main coupling and cross-coupling signals cancel at the location of the full mode capacitively loaded SIW resonator, where the transmission zero (TZ) was generated.

3. Wide stopband response

This design employs S-HCMSIW resonator and full mode capacitively loaded SIW resonator. Both resonators are loaded with different amounts of inductance and capacitance, which results in a different distribution of modes with respect to frequency. To further compre-

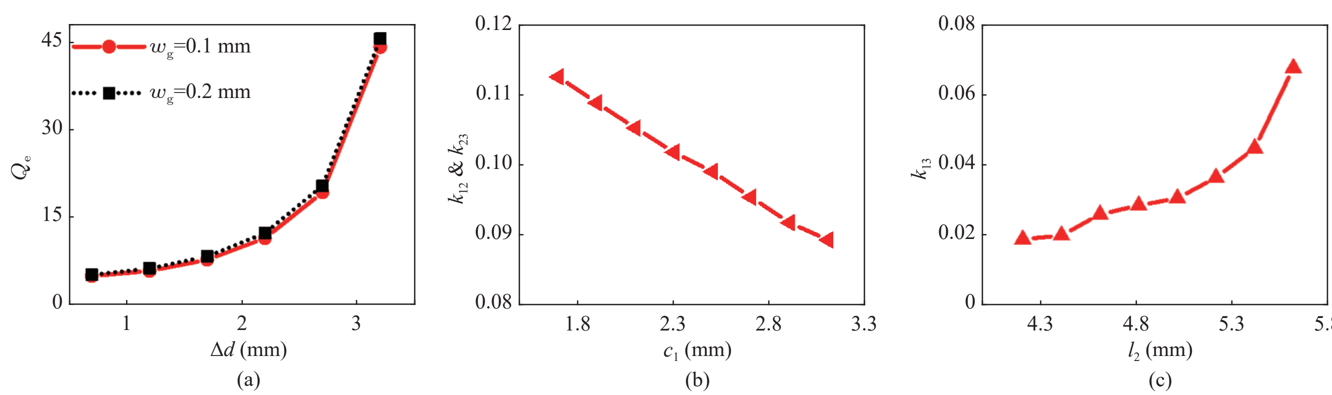

Figure 4 (a) Simulated external quality factor Q_e by varying w_g and Δd; (b) Coupling coefficient k_{12} & k_{23} versus c_1; (c) Coupling coefficients k_{13} versus l_2.

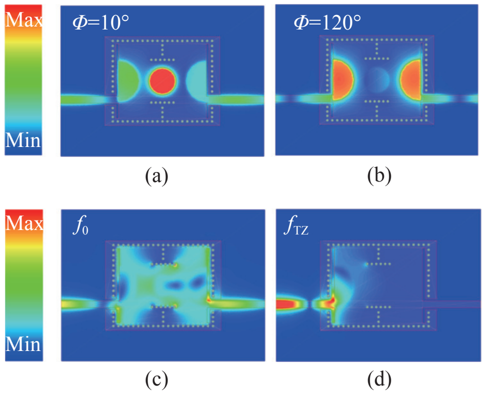

Figure 5 (a) and (b): Electric field distributions of the proposed filter at f_0 for different phases; (c) and (d): Magnetic field distributions of the proposed filter at f_0 and f_{TZ}.

hend the impact of the resonators on the response of this filter, we studied the mode versus frequency distribution for both resonators and plotted the results in Figure 6, where $f_{R1\&R3,n}$ and $f_{R2,n}$ indicate the mode of S-HCMSIW resonator and the full mode capacitively loaded SIW resonator, respectively. It is worth noting that when n is 0, it means that its fundamental mode. The higher modes of the two resonators do not occur at the same frequency, except for the fundamental mode, which results in a wide stopband response on the right side of the passband, as depicted in the figure. And the full mode capacitively loaded SIW resonator investigated resulting in an even wider stopband compared to the S-HMCSIW resonators for it loaded with larger inductor.

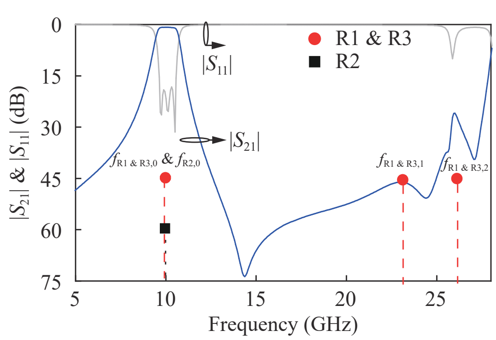

Figure 6 Higher order modes frequency distribution of the R1 & R3 (S-HCMSIW resonator), R2 (full mode capacitively loaded SIW resonator).

IV. Fabrication and Measurement

The design is implemented with the parameters shown in Table 2, and the measured results are compared with the simulation results to validate the earlier study. This filter utilizes the RT/Duroid 5880 (dielectric constant of 2.2) as the substrate material and copper as the metal material. Figure 7(a) displays a comparison graph of the simulated, test results and the coupling matrix synthesized response. The group delay for the proposed filter was shown in Figure 7(b). As shown by Figure 7(c), the structure's two layers are manufactured independently and connected by nylon screws.

Table 2 Design geometrical parameters (Units: mm)

w_1	l_1	c_1	c_2	l_2	m	w_g
5.6	8.57	2.5	2.13	4.82	0.31	0.2
d_1	d_2	d_3	d	f	Δd	–
1.4	0.94	2.55	0.2	0.77	2.2	–

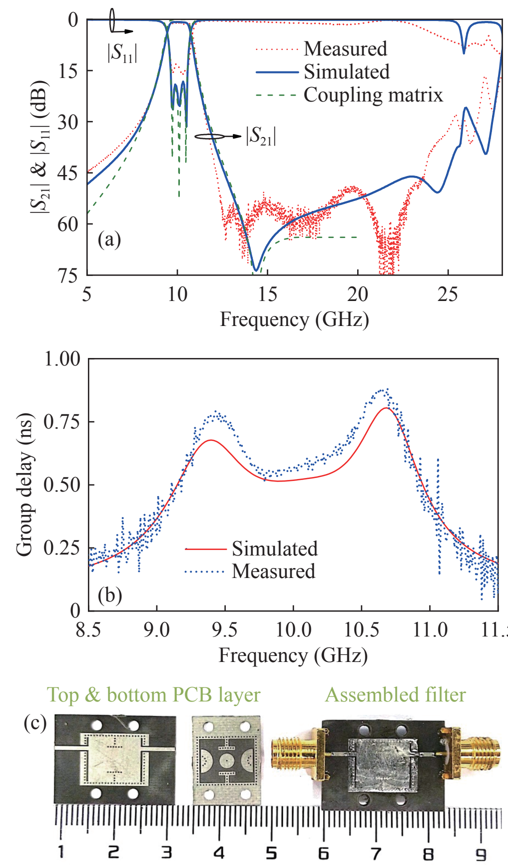

Figure 7 (a) Simulated, measured and coupling matrix fitted wideband $|S_{21}|$ and $|S_{11}|$ for the proposed filter; (b)The group delay for the proposed filter; (c) The photo of the manufactured filter.

The slight discrepancy is mainly caused by the manufacturing tolerance. The center frequency of the filter is 10 GHz with the lowest in-band loss being 1.09 dB, and its relative bandwidth (FBW) is 16.2%.

This design's superiority is demonstrated in Table 3 by comparing it with other designs on a variety of attributes. Due to their exposed radiation surface, HMSIW-based filters in [8] and [14] have a substantial insertion loss. The microstrip BPF with in-line topology has been studied in [26]. It has a rather substantial insertion loss and an unsatisfactory stopband rejection. The filters described in [27] and [28] were designed for signal transmission by cascading or stacking in the plane of the cavities. Their size is large with poor stopband rejection.

V. Conclusion

By shielding the half-mode capacitively-loaded cavity resonator, a new type of resonator is proposed in this ar-

Table 3 Comparison with the past related works

Ref.	Type	Frequency (GHz)	IL (dB)	3-dB FBW (%)	Stopband rejection level	Electrical size ($\lambda_0 \times \lambda_0$)
[8]	HMSIW	10	2.4	5.3	$1.05f_0$ @30 dB	1.64 × 0.92
[14]	HMSIW	10.71	1.57	10	$1.57f_0$ @20 dB	0.84 × 0.38
[26]	Microstrip	3	1.43	8.3	$1.4f_0$ @20 dB	0.32 × 0.13
[27]	SIW	6.5	2.52	1.92	$2.51f_0$ @25 dB	1.06 × 0.92
[28]	SIW	8.5	1.7	6.12	$2.08f_0$ @20 dB	1.1 × 1.05
This work	Capacitively loaded SIW	10	1.09	16.2	$2.35f_0$ @45 dB & $2.69f_0$ @20 dB	0.39 × 0.51

ticle. This S-HCMSIW resonator is promising for application in wireless systems due to its high Q and miniaturization characteristics. Later, we designed a third-order filter by combining two S-HMCSIW resonators with a full mode capacitively loaded resonator. By incorporating a TZ, the structure improves the roll-off characteristics of the passband. Meanwhile, the stopband is widened by the resonator forms of different sizes. The proposed technique can be extended to develop other X-band passive and active microwave/millimeter-wave components with desired superior characteristics.

References

[1] X. L. Yang, X. W. Zhu, and X. Wang, "Dual-band substrate integrated waveguide filters with perturbed circular cavity," *IEEE Microwave and Wireless Components Letters*, vol. 32, no. 4, pp. 293–296, 2022.

[2] G. Zhang, J. Zheng, X. Y. Zhang, *et al.*, "Dual-band balanced to unbalanced multilayer filtering magic-T based on SIW Cavity," *IEEE Microwave and Wireless Components Letters*, vol. 32, no. 5, pp. 387–390, 2022.

[3] Y. L. Zhu, Y. D. Dong, X. Luo, *et al.*, "Dual-band SIW filter with widely separated passbands based on TE101 and TE301 modes," in *2022 IEEE/MTT-S International Microwave Symposium-IMS 2022*, Denver, CO, USA, pp.464–467, 2022.

[4] A. Iqbal, A. W. Ahmad, A. Smida, *et al.*, "Tunable SIW bandpass filters with improved upper stopband performance," *IEEE Transactions on Circuits and Systems II:Express Briefs*, vol. 67, no. 7, pp. 1194–1198, 2020.

[5] A. Iqbal, J. J. Tiang, C. K. Lee, *et al.*, "Dual-band half mode substrate integrated waveguide filter with independently tunable bands," *IEEE Transactions on Circuits and Systems II:Express Briefs*, vol. 67, no. 2, pp. 285–289, 2020.

[6] F. Zhu, Y. F. Wu, P. Chu, *et al.*, "Single-layer substrate-integrated waveguide inline filters with flexible transmission zeros," *IEEE Microwave and Wireless Components Letters*, vol. 32, no. 6, pp. 495–498, 2022.

[7] A. Iqbal, J. J. Tiang, S. K. Wong, *et al.*, "QMSIW-based single and triple band bandpass filters," *IEEE Transactions on Circuits and Systems II:Express Briefs*, vol. 68, no. 7, pp. 2443–2447, 2021.

[8] F. Zhu, G. Q. Luo, Z. Liao, *et al.*, "Compact dual-mode bandpass filters based on half-mode substrate-integrated waveguide cavities," *IEEE Microwave and Wireless Components Letters*, vol. 31, no. 5, pp. 441–444, 2021.

[9] G. J. Wen, J. Li, F. Z. Xie, *et al.* , "Millimeter-wave SIW filter based on the stepped-impedance face-to-face E-shaped DGSs," in *2019 IEEE MTT-S International Microwave Symposium (IMS)*, Boston, MA, USA, pp.830–833, 2019.

[10] B. K. Jin, P. J. Zhang, J. D. Mu, *et al.*, "A miniaturized bandpass filter basing on HMSIW loaded dual-mode CSRR," in *2021 IEEE MTT-S International Wireless Symposium (IWS)*, Nanjing, China, pp.1–3, 2021.

[11] T. R. Jones and M. Daneshmand, "Miniaturized folded ridged half-mode and quarter-mode substrate integrated waveguides for filter design," *IEEE Transactions on Microwave Theory and Techniques*, vol. 67, no. 8, pp. 3414–3426, 2019.

[12] L. W. Huang and S. F. Zhang, "Ultra-wideband ridged half-mode folded substrate-integrated waveguide filters," *IEEE Microwave and Wireless Components Letters*, vol. 28, no. 7, pp. 579–581, 2018.

[13] P. Chu, J. G. Feng, L. Guo, *et al.*, "Multilayer substrate integrated waveguide filter with multimode suppression and wide stopband," *IEEE Transactions on Circuits and Systems II:Express Briefs*, vol. 69, no. 11, pp. 4553–4557, 2022.

[14] L. Gu and Y. D. Dong, "Compact half-mode SIW filter with high selectivity and improved stopband performance," *IEEE Microwave and Wireless Components Letters*, vol. 32, no. 9, pp. 1039–1042, 2022.

[15] H. W. Deng, Y. K. Han, L. Sun, *et al.*, "Multilayer dual-mode balanced SIW filter utilizing PEC–PMC characteristic for common-mode suppression," *IEEE Microwave and Wireless Components Letters*, vol. 30, no. 9, pp. 865–868, 2020.

[16] M. K. Li, Q. Ji, C. Chen, *et al.*, "A triple-mode bandpass filter with controllable bandwidth using QMSIW cavity," *IEEE Microwave and Wireless Components Letters*, vol. 28, no. 8, pp. 654–656, 2018.

[17] P. Chu, L. Guo, L. Zhang, *et al.*, "Wide stopband substrate integrated waveguide filter implemented by orthogonal ports' offset," *IEEE Transactions on Microwave Theory and Techniques*, vol. 68, no. 3, pp. 964–970, 2020.

[18] Y. L. Zhu and Y. D. Dong, "A compact dual-band quasi-elliptic filter based on hybrid SIW and microstrip technologies," *IEEE Transactions on Circuits and Systems II:Express Briefs*, vol. 69, no. 3, pp. 719–723, 2022.

[19] G. Lin, Y. D. Dong, and X. Luo, "Miniaturized quarter-mode SIW filters loaded by dual-mode microstrip resonator with high selectivity and flexible response," *IEEE Microwave and Wireless Components Letters*, vol. 32, no. 6, pp. 660–663, 2022.

[20] J. Zhou, Y. B. Rao, D. X. Yang, *et al.*, "Compact wideband BPF with wide stopband using substrate integrated defected ground structure," *IEEE Microwave and Wireless Components Letters*, vol. 31, no. 4, pp. 353–356, 2021.

[21] J. C. Xie, D. S. Tang, Y. Y. Shu, *et al.*, "Compact UWB BPF with broad stopband based on loaded-stub and C-shape SIDGS resonators," *IEEE Microwave and Wireless Components Letters*, vol. 32, no. 5, pp. 383–386, 2022.

[22] J. S. Hong and M. J. Lancaster, *Microstrip Filters for RF/Microwave Applications*. Wiley, New York, NY, USA, pp.8–10, 2001.

[23] A. Iqbal, A. Smida, M. I. Waly, *et al.*, "Highly-tunable and wide stopband microstrip bandpass filters," *International Journal of RF and Microwave Computer-Aided Engineering*, vol. 31, no. 5, article no. e22610, 2021.

[24] L. Q. Li, H. R. Zhu, X. Y. Ning, *et al.*, "A Miniaturized bandwidth reconfigurable bandpass chip filter with semi-lumped topology and GaAs pHEMT technology," *Chinese*

Journal of Electronics, vol. 30, no. 1, pp. 192–198, 2021.

[25] J. F. Chen, F. C. Chen, R. S. Li, *et al.*, "High selectivity cascaded quadruplet bandpass filter with three pairs of transmission zeros," *Chinese Journal of Electronics*, vol. 26, no. 5, pp. 1101–1104, 2017.

[26] Y. Wu, K. X. Ma, and Y. Q. Wang, "Design of in-line filter with cross-couplings paths and source loaded dangling resonator produced transmission zeros," in *2022 IEEE/MTT-S International Microwave Symposium-IMS 2022*, Denver, CO, USA, pp.460–463, 2022.

[27] H. W. Xie, K. Zhou, C. X. Zhou, *et al.*, "Wide-stopband SIW filters using modified multi-spurious modes suppression technique," *IEEE Transactions on Circuits and Systems II:Express Briefs*, vol. 67, no. 12, pp. 2883–2887, 2020.

[28] W. Shen and H. R. Zhu, "Vertically stacked trisection SIW filter with controllable transmission zeros," *IEEE Microwave and Wireless Components Letters*, vol. 30, no. 3, pp. 237–240, 2020.

Yan ZHENG received the B.E. degree in measurement and control technology and instrument from the Henan University, Kaifeng, in 2018, and the M.S. degree in electronics and communication engineering from the University of Electronic Science and Technology of China (UESTC), Chengdu, in 2022. She is currently pursuing the Ph.D. degree in electromagnetic field and microwave techniques at UESTC. Her research interests include the synthesis design of planar microwave, integrated passive device filters, and acoustic-wave filters for wireless communication applications.
(Email: iszhengyan@163.com)

Hanyu TIAN is currently pursuing the Ph.D. degree in electronic science and technology at the University of Electronic Science and Technology of China, Chengdu, China. His research interests include multifunctional filtering components, filtering power dividers, and the filter synthesis techniques. He was a recipient of the IEEE IWS Best Student Paper Award Finalist in 2021.
(Email: hanyutian@std.uestc.edu.cn)

Yuandan DONG received the B.S. and M.S. degrees from the Department of Radio Engineering, Southeast University, Nanjing, China, in 2006 and 2008, respectively, and the Ph.D. degree from the Department of Electrical Engineering, University of California at Los Angeles (UCLA), Los Angeles, CA, USA, in 2012.

From September 2008 to June 2012, he was a Graduate Student Researcher with the Microwave Electronics Laboratory, UCLA. From September 2012 to February 2016, he was working as a Senior Engineer with the Research and Development Hardware Department, Qualcomm, San Diego, CA, USA. From February 2016 to December 2017, he was working as a Staff Engineer with Universal Electronics Inc., Santa Ana, CA, USA. Since December 2017, he has been a Full Professor with the University of Electronic Science and Technology of China (UESTC), Chengdu, China. He has authored or coauthored more than 260 journal articles and conference papers, which receive more than 5600 citations. He has been listed as an Elsevier highly cited researcher. He holds more than 100 patents including six international patents. He and his team have developed multiple RF products including acoustic wave filters, antenna tuners, and antennas, which are very widely shipped and applied in mobile devices. His research interests include the characterization and development of RF and microwave components, antennas, RF frontend modules, circuits, acoustic-wave filters, and metamaterials.

Dr. Dong was a recipient of the Best Student Paper Award from 2010 IEEE Asia Pacific Microwave Conference (APMC) held in Yokohama, Japan, the Best Paper Award in 2021 and 2023 IEEE International Wireless Symposium (IWS), the Distinguished Expert Presented by Sichuan Province and by the national government, respectively, and the High Level Innovative and Entrepreneurial Talent presented by Jiangsu Province. He has been a TPC member for several international conferences. He has served as an Associate Editor for the *IEEE Transactions on Antennas and Propagation* since 2021. And he has served as a guest editor for *IEEE Open Journal of Antennas and Propagation*. He is also serving as a Reviewer for multiple IEEE and IET journals including the *IEEE Transactions on Microwave Theory and Techniques* and the *IEEE Transactions on Antennas and Propagation*. (Email: ydong@uestc.edu.cn)